Journal of Cellular Biochemistry

WILEY

Journal of Cellular Biochemistry

RESEARCH ARTICLE OPEN ACCESS

Transforming Growth Factor-β Modulates Cancer Stem Cell Traits on CD44 Subpopulations in Hepatocellular Carcinoma

Mario Alejandro Aguilar-Chaparro[1] | Sonia Andrea Rivera-Pineda[1] | Hury Viridiana Hernández-Galdámez[1] | Emmanuel Ríos-Castro[2] | Olga Lilia Garibay-Cerdenares[3] | Carolina Piña-Vázquez[1] | Saúl Villa-Treviño[1]

[1]Departamento de Biología Celular, Centro de Investigación y de Estudios Avanzados del IPN (CINVESTAV), México City, México | [2]Laboratorios Nacionales de Servicios Experimentales, Centro de Investigación y Estudios Avanzados del IPN, Ciudad de México, México | [3]CONAHCyT- Universidad Autónoma de Guerrero, Chilpancingo, México

Correspondence: Saúl Villa-Treviño (svilla@cinvestav.mx)

Received: 26 September 2024 | **Revised:** 29 December 2024 | **Accepted:** 25 January 2025

Keywords: cancer stem cells | CD44 isoforms | epithelial-mesenchymal transition | hepatocellular carcinoma | transforming growth factor-beta

ABSTRACT

Hepatocellular carcinoma (HCC) is a formidable malignancy, with growing interest in identifying cancer stem cells (CSCs) as potential therapeutic targets. CD44 isoforms have emerged as promising CSC markers in HCC, often associated with epithelial-mesenchymal transition (EMT) induced by transforming growth factor-beta (TGF-β). However, the intricate relationship between CSC traits, CD44 isoforms, and TGF-β effects on CD44 subpopulations in HCC remains unclear. This study aimed to clarify how TGF-β influences proteomic changes and CSC traits in subpopulations expressing standard CD44 isoform (CD44std) and CD44 variant 9 (CD44v9). Treating SNU-423 cells with TGF-β lead to notable morphological changes, resembling a spindle-like phenotype, along with reductions in CD44v9+ subpopulations and differential CD44std expression. Proteomic analysis highlighted significant alterations in signaling pathways, particularly the mitogen-activated protein kinase (MAPK) pathway. Validation experiments demonstrated upregulation in CD44std cells and downregulation in CD44v9 cells post-TGF-β treatment. Furthermore, TGF-β exerted regulatory influence over Sox2 and Nanog expression, resulting in increased colony and spheroid formation in CD44std cells but decreased capabilities in CD44v9 cells. TGF-β also enhanced the migratory and invasive properties of both subpopulations through EMT, alongside increased adhesive abilities in CD44v9 cells. These findings illuminate the dynamic interplay between TGF-β and CD44std/CD44v9 subpopulations, emphasizing the role of MAPK signaling and modulation of CSC traits. This research contributes to understanding the dynamic interplay between CD44 isoforms and TGF-β in HCC.

1 | Introduction

Liver cancer presents a global and continuously escalating challenge, with projections indicating that by 2025, the disease will afflict one million people. This type of cancer ranks third among the most lethal cancers, surpassed only by stomach cancer and lung cancer [1, 2]. Worldwide, approximately 90% of liver cancer cases are diagnosed as hepatocellular carcinoma (HCC), with an annual incidence of 800 000 cases [3]. CD44 is a hyaluronic acid (HA) receptor and a marker for CSCs across various cancer types. It stands out in the literature for its capacity for isoform generation through alternative splicing [4, 5]. These isoforms include standard CD44 (CD44std), with a molecular weight of 85 kDa and lacking variable exons, and variant CD44 (CD44v) isoforms, which have molecular weights of 100 to 250 kDa and may include individual or grouped exons,

such as v2-10 [6]. In the context of HCC, a connection has been established between the expression of the CD44std isoform and CD44v5, v6, v7-8, and v10 and unfavorable prognosis and metastasis [7]. Importantly, the majority of studies have linked the expression of CD44std with the induction of epithelial-mesenchymal transition (EMT) [8]. While CD44v6 has been associated with invasive characteristics in in vitro studies, knowledge about its clinical relevance is limited [9]. Previously, we reported the presence of the CD44std and CD44v9 subpopulations in SNU-423 cells, which were isolated by a CD44v9 MACS system, where we observed differential CSC features [10].

One of the known inducers of EMT is transforming growth factor beta (TGF-β), which triggers the expression of CD44std via epithelial splicing regulatory proteins (ESRPs) [11]. However, the relationship among TGF-β, CD44 isoforms, and CSC characteristics in HCC remains incompletely understood. A study assessing the impact of inhibition of CD44std blocked TGF-β-induced EMT. In clinical terms, the expression of CD44std in HCC tumors has been linked to a more mesenchymal profile and an unfavorable prognosis [12]. Additionally, the presence of CD44std in HCC has been identified to contribute to both EMT and spheroid formation. However, most studies have focused on the role of CD44std in TGF-β-mediated EMT [12], leaving a gap in our understanding of the behavior of CD44v isoforms and their implications for CSC characteristics.

Therefore, we conducted an analysis of proteomic changes and the modulation of CSC characteristics in the CD44std and CD44v9 subpopulations following treatment with TGF-β. Morphological changes, characterized by a shift toward a spindle-shaped morphology, were observed in CD44std and CD44v9 cells after treatment with TGF-β. This was accompanied by a decrease in the CD44v9+ subpopulation and differential expression of CD44std. Proteomic analysis revealed a significant alteration in the MAPK signaling pathway, which was upregulated in CD44std cells and downregulated in CD44v9 cells, as subsequently confirmed. In addition, the clonogenicity and spheroid characteristics of CD44std and CD44v9 cells were modulated, along with increases in migratory and invasive behaviors in CD44std cells and in adhesive behavior in CD44v9 cells. These results underscore how different proteins in the MAPK signaling pathway lead to changes in phenotype, such as those observed in the CD44std and CD44v9 subpopulations after treatment with TGF-β, and can be potential targets for suppressing the development of HCC.

2 | Materials and Methods

2.1 | Cell Culture

SNU-423 cells were cultured following the instructions provided by American Type Culture Collection in Roswell Park Memorial Institute 1640 (RPMI 1640) medium supplemented with 10% decomplemented fetal bovine serum (FBS) and antibiotics (ampicillin and streptomycin) in a humidified environment at 37°C and 5% CO_2.

2.2 | TGF-β Treatment

After separating CD44v9 subpopulations of SNU-423 cells using MACS, the CD44std and CD44v9 subpopulations were either left untreated (NT) in complete RPMI 1640 medium or treated with TGF-β (T) (Cat# 100-21; PeproTech) at a concentration of 2 ng/mL for 72 h.

2.3 | Flow Cytometry

A total of 1×10^6 CD44std and CD44v9 cells were incubated with a panspecific Alexa Fluor 700-conjugated α-CD44 antibody (1:500; Cat. No. 561289) in the dark for 20–30 min at 4°C. After α-CD44v9 antibody treatment (1:300; Cosmo Bio Co. Ltd.; Cat. No. LKG-M001), the CD44v9-labeled cells were subsequently incubated with a FITC-conjugated α-rat secondary antibody (1:2000; Invitrogen; Cat. No. 31629). After incubation, the cells were centrifuged at 2000 rpm for 5 min, washed twice with PBS 1× containing 2% FBS, and then resuspended at 4°C. Subsequently, the cells were analyzed using a CytoFLEX-LX flow cytometer and CytExpert 2.1 software. A total of 15 000 events were acquired, and dead cells stained with propidium iodide and cellular debris were excluded from the population analysis.

2.4 | Western Blot Analysis

Total protein extraction was carried out using RIPA lysis buffer containing 100 μL/mL protease inhibitor cocktail (cOmplete, Roche Applied Science, Mannheim, Germany) and 10 μL/mL phosphatase inhibitor (PhosSTOP, Roche Applied Science, Mannheim, Germany). Equal amounts of protein (20-30 μg) were loaded onto an 8-10% SDS–PAGE gel and separated at 80 V for 30 min. Subsequently, the voltage was increased to 120 V for 2 h. Protein integrity was verified by Coomassie blue staining. Next, the SDS–PAGE gel was equilibrated for 10 min before transferring the proteins to a polyvinylidene fluoride (PVDF) membrane. Protein transfer from the gel to the PVDF membrane was carried out at 0.3 A for 2 h, and the membrane was then incubated with Ponceau red to verify protein transfer. Membrane blocking was achieved using low-fat milk diluted in 1× TBS or PBS with Tween 20. The membrane was then incubated with α-CD44 (1:8000; Abcam; Cat. No. ab189524), α-GAPDH (1:10 000; Cell Signaling Technologies; Cat. No. 5174), α-Oct-4A (1:500; Cell Signaling Technologies; Cat. No. 5174), α-Sox2 (1:500; Cell Signaling Technologies; Cat. No. 3579), α-Nanog (1:500; Cell Signaling Technologies; Cat. No. 8822), α-N-Cadherin (1:1000; Santa Cruz; Cat. No. 13A9), α-vimentin (1:1000; Santa Cruz; Cat. No. sc-6260), α-E-cadherin (1:1000; Abcam; Cat. No. Sc-21791), α-Scr (1:1000; Cell Signaling Technologies; Cat. No. 36D10), α-MEK (1:1000; GeneTex; Cat. No. GTX50313), α-MAPK (1:1000; Cell Signaling Technologies; Cat. No. 9102) and α-p-MAPK (1:1000; Cell Signaling Technologies The following day, the membrane was washed three times with TBS or PBS 1× with Tween 20 before incubation with the corresponding mouse or rabbit secondary antibody for 1 h at room temperature. After three washes with the appropriate solution, the membrane was incubated with luminol (Millipore).

2.5 | Sample Preparation for Mass Spectrometry

Protein extraction from the CD44std and CD44v9 subpopulations after treatment was performed using RIPA buffer, and a protease inhibitor cocktail was added to maintain protein integrity. Equal amounts of protein were prepared for proteomic analyses. For each biological sample (CD44std and CD44v9 subpopulations, NT, and T), 1×10^6 cells were collected, washed, and centrifuged. The protein homogenate was incubated for 30 min at 4°C and then centrifuged at 12 000 rpm and 4°C for 20 min. The supernatant was recovered and quantified. Protein concentrations were measured using the Lowry method, and 20 μg of protein was used for each condition and each biological replicate. Proteins were separated by 10% SDS–PAGE, and Coomassie blue staining was performed to visualize sample integrity. The protein samples were processed for mass spectrometry according to a standard protocol. The protein samples were digested by incubation with 50 μL of a Lys-C/trypsin mixture ("Digest" reagent) at 37°C for 2 h. The resulting peptides were cleaned using an iST cartridge with Wash Buffer 1 to remove hydrophobic contaminants and Wash Buffer 2 to remove hydrophilic contaminants. Subsequently, the peptides were eluted using an elution reagent and then dried in a SpeedVac. Finally, the peptides were resuspended with LC–Load reagent and stored at −80°C until analysis by LC–MS.

2.6 | Label-Free DIA Mass Spectrometry Analysis

Quantitative proteomic analysis (spectrometric and chromatographic conditions) was performed using a UPLC Nano Acquity M-Class system coupled to a QTOF SYNAPT G2-Si mass spectrometer (Waters; Milford, MA, USA) following the method of Emmanuel Rios, 2020 [13]. The generated *.raw files were analyzed using Progenesis QI for Proteomics v3.0.3 software (Waters; Milford, MA, USA) according to specified scenarios, with the following modifications: we used a concatenated *.fasta database of *Homo sapiens* (obtained from UniProt, containing 73 099 protein sequences, last updated on October 11, 2022). Calibration of SYNAPT G2-Si was performed with [Glu1]-fibrinopeptide fragments through precursor ion ($[M + 2H]2+ = 785.84261$) fragmentation at 32 eV, resulting in a deviation of less than 1.1 ppm in all MS/MS measurements. Ratios were calculated based on the average MS signal response of the three most intense tryptic peptides (Top3) for each characterized protein in CD44std and CD44v9 samples treated with TGF-β (T) relative to the Top3 for each protein in untreated CD44std and CD44v9 samples.

2.7 | Bioinformatics Analysis

The proteomic data were analyzed using Excel files named CD44std NT versus CD44std TGF-β and CD44v9 NT versus CD44v9 TGF-β. The proteomic data were subjected to filtering and visualization on a volcano plot generated using the VolcaNoseR server, accessible online (https://huygens.science.uva.nl/VolcaNoseR/; accessed on May 15 2023). Differential expression profiles were assessed using a heatmap generated by the Heatmapper web server, available online (http://heatmapper.ca/; accessed on May 28 2023), with complete linkage clustering and the Pearson distance method employed. Differentially expressed proteins were classified according to biological pathways using the Reactome Pathway database within STRING v11 (available online: https://string-db.org/; accessed on June 8 2023). Unique proteins specific to the CD44std NT versus CD44std TGF-β and CD44v9 NT versus CD44v9 TGF-β comparison groups were identified based on analysis of the filtered protein data of these groups. A Venn diagram was generated using the Venny 2.0 server, available online (https://bioinfogp.cnb.csic.es/tools/venny/; accessed on June 12 2023). These unique proteins were combined with the differentially expressed proteins in the CD44std NT versus CD44std TGF-β and CD44v9 NT versus CD44v9 TGF-β comparison groups. The identified proteins were subjected to analysis using the Gene Ontology (GO) platform, available online (http://geneontology.org/; accessed on June 15 2023), focusing on biological pathways, signaling, intracellular signal transduction, and information. The selected proteins were analyzed with STRING (https://string-db.org/, accessed on June 18 2023), which is a highly useful tool for the analysis of molecular interaction networks between proteins. All identified biological pathways with a false discovery rate (FDR) of < 0.05 were considered highly reliable and were exported as a file. The interactomes of the differentially expressed proteins were generated in STRING, with configuration settings including the *Homo sapiens* database; text mining, experiments, databases, coexpression, neighborhood, gene fusion, and co-occurrence as active interaction sources; and a minimum confidence score of 0.4.

2.8 | Clonogenicity Assay

In 6-well plates, 500 cells were seeded per well and cultured at 37°C in a humidified atmosphere with 5% CO_2. After 14 days of culture, the number of colonies was determined. At the conclusion of the experiment, the cells were washed twice with PBS 1×, fixed with 4% paraformaldehyde for 15 min, and stained with 0.5% crystal violet for 5 min. The analysis involved counting the colonies consisting of a minimum of 50 cells.

2.9 | Spheroid Formation Assay

In 24-well low-adhesion plates, 500 cells were seeded per well and cultured in serum-free DMEM/F12 medium (Gibco) supplemented with 20 ng/mL recombinant human epidermal growth factor (rhEGF; Invitrogen), 10 ng/mL recombinant human basic fibroblast growth factor (rhbFGF; Invitrogen), and 2% B27 supplement without vitamin A (Invitrogen). The culture was maintained for 15 days at 37°C in a humidified atmosphere with 5% CO_2. The cells were monitored over the course of 7–15 days.

2.10 | Wound Healing Migration Assay

In 24-well plates, 1×10^5 cells were seeded per well and allowed to grow until they were completely confluent or formed a cell monolayer. Subsequently, the cells were serum-starved for 12 h and treated with 14 μg of mitomycin for 2 h to prevent cell

growth. A wound was created by gently scratching the monolayer in a straight line using a 1000 μL pipette tip. Next, the cells were washed with PBS 1× to remove detached cells, and fresh medium was added. Wound closure was evaluated at different time points (0, 24, and 48 h) and documented through photography using an optical microscope (Olympus IX70).

2.11 | Adhesion Assay

The wells of 96-well plates pretreated with 20 μg/mL fibronectin (Invitrogen) for 2 h at 37°C in a 5% CO_2 atmosphere were washed with PBS 1× and incubated with 0.5% BSA-containing medium to block nonspecific binding. Next, 5×10^4 cells were seeded per well in triplicate, and the plates were incubated for 40 min at 37°C in a 5% CO_2 atmosphere. Subsequently, the medium was removed, and the cells were washed three times with PBS 1×, fixed with methanol for 15 min, stained with crystal violet for 5 min, and photographed using an optical microscope (Olympus IX 70). Finally, the cells were solubilized in PBS 1× containing 2% SDS, and the absorbance was measured at 550 nm.

2.12 | Transwell Invasion Assay

The cell invasion assay was conducted using BD Transwell chambers with 8 μm filter membranes. The membranes were coated with Matrigel Matrix Basement Membrane (Corning; Ref. No. 356237) following the manufacturer's instructions. Cells (1×10^5 per well) were seeded in the upper inserts on the Matrigel layer in serum-free medium, while 500 μL of medium supplemented with 10% serum was added to the lower compartments. The plates were incubated for 48 h at 37°C in a 5% CO_2 atmosphere. Then, the cells were fixed with cold methanol for 5 min, and the medium was removed from the insert. The cells were stained with crystal violet, followed by multiple washes with MQ H2O.

2.13 | Statistical Analysis

Data analysis was conducted using GraphPad PRISM version 6.01 software. The data are graphically presented and expressed as the mean ± standard deviation of three independent experiments. The significance of differences between two groups was determined using Student's *t*-test, while ANOVA was employed to assess the significance of differences among multiple experimental groups. A p value of less than *0.05* was considered to indicate a statistically significant difference.

3 | Results

3.1 | TGF-β Induces Morphological Changes and Alters CD44std and CD44v9 Expression

We isolated the CD44std (12.8%) and CD44v9 (99.7%) subpopulations of SNU-423 cells using a MACS CD44v9 system as previously reported [10]. Consecutively, it was decided to evaluate the effect of TGF-β (2 ng/mL) treatment or no treatment (RPMI medium) for 72 h. We investigated the morphological changes induced by TGF-β in these subpopulations (Figure 1A). CD44std cells exhibited a spindle-shaped morphology, whereas CD44v9 cells exhibited both a polygonal and a spindle-shaped morphology. Following TGF-β treatment for 72 h, a shift toward a spindle-shaped morphology was induced in both subpopulations. Measurement of the cellular area index showed a significant increase in the relative area after TGF-β treatment. Flow cytometric analysis of the CD44v9 subpopulation revealed no difference in the CD44std cells but a decrease in the CD44v9 cells following TGF-β treatment (Figure 1B). To confirm the identity of the CD44 isoforms expressed in the CD44std and CD44v9 subpopulations after TGF-β treatment, we assessed total CD44 expression by Western blot (WB) analysis using a panspecific anti-CD44 antibody. CD44std cells showed reduced CD44std and CD44v expressions, while CD44v9 cells exhibited increased CD44std expression and no changes in CD44v expression (Figure 1C). These findings demonstrate that TGF-β modifies the spindle-shaped cell morphology and decreases the CD44v9 subpopulation while altering the expression of CD44std in the CD44std and CD44v9 cell subpopulations. These findings demonstrate that TGF-β modifies the spindle-shaped cell morphology, decreases the CD44v9+ subpopulation and alters CD44std expression in the CD44std and CD44v9 subpopulations.

3.2 | TGF-β Stimulation Elicits Differential Alterations in the MAPK Signaling Pathway in CD44std and CD44v9 Cells

Four conditions (with and without TGF-β stimulation in the CD44std and CD44v9 subpopulations) were analyzed to understand the effect of TGF-β stimulation and the phenotypic changes induced by TGF-β. For the 11 305 quantified proteins shared between the untreated (NT) and TGF-β-treated (T) conditions, we applied filtering criteria (CV < 0.30, at least two peptides per protein, considering at least one unique peptide, identified in 3/3 samples, and $p < 0.05$ by ANOVA) and excluded "reversed" protein sequences. On a volcano plot with a cutoff value of 1, the proteins were distributed, and their expression levels were expressed as logarithm base 2 (log2) values. We identified 398 upregulated proteins, 109 downregulated proteins and 3,830 proteins with no change in expression in CD44std cells after TGF-β stimulation. In CD44v9 cells after TGF-β stimulation, 147 proteins were upregulated, 238 were downregulated and 3,745 were unchanged (Supporting Information S1: Figure S1A). The differential expression analysis results were visualized on a heatmap, which revealed distinct protein expression profiles between CD44std and CD44v9 cells (Supporting Information S1: Figure S1B). We then explored the proteins present exclusively in the CD44std and CD44v9 subpopulations using a Venn diagram after removing the 4,108 proteins shared between the two subpopulations from the filtered protein data from CD44std (4,337 proteins) and CD44v9 (4,130 proteins) cells. CD44std cells contained 229 exclusive proteins, while CD44v9 cells had 22 exclusive proteins in the untreated condition. Additionally, 507 upregulated and downregulated proteins were added to CD44std cells, while 385 upregulated and downregulated proteins were added to CD44v9 cells after TGF-β treatment, for a total of 736 differentially expressed proteins in CD44std cells and 407 in CD44v9 cells (Supporting Information S1: Figure S2). These proteins were subjected to GO analysis, focusing on biological processes and

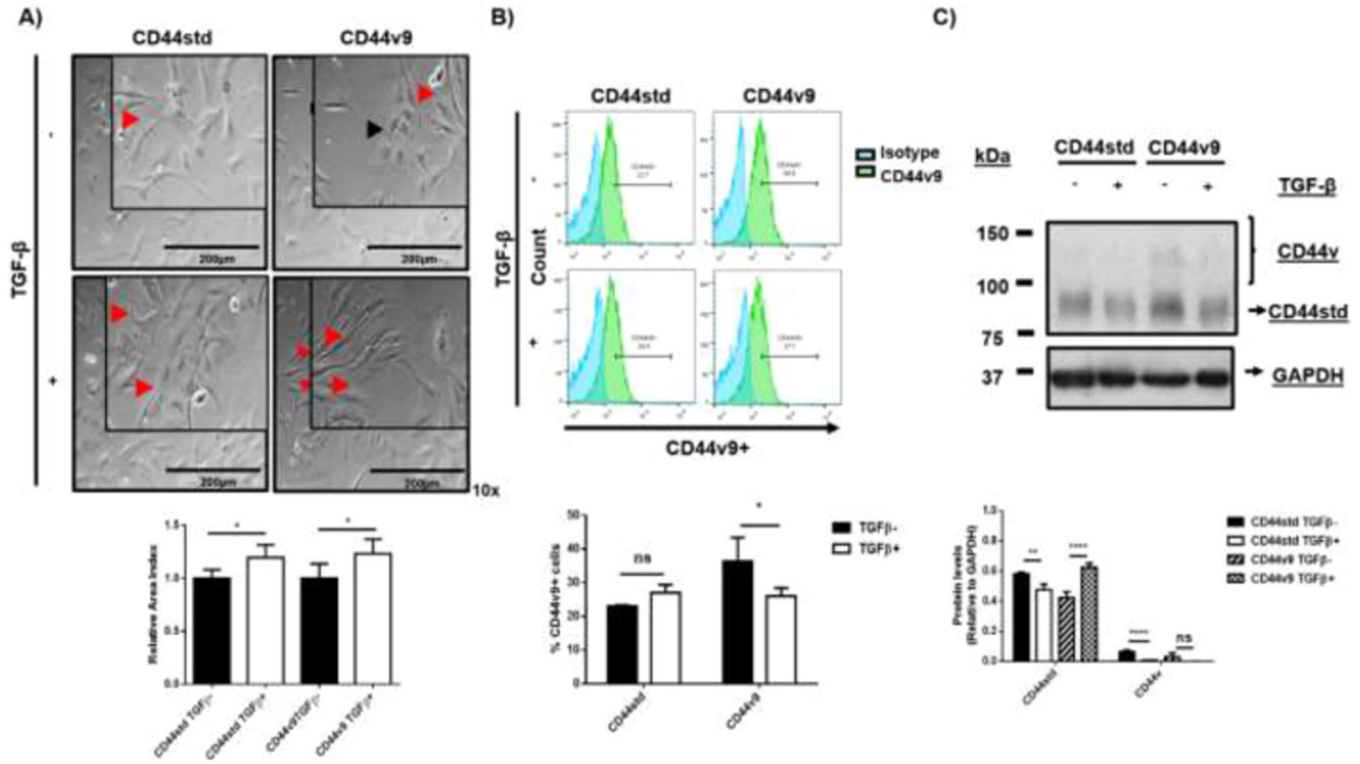

FIGURE 1 | Effects of TGF-β on morphological changes and CD44 isoform expression changes in the CD44std and CD44v9 subpopulations. (A) Morphological changes in the CD44std and CD44v9 subpopulations 72 h after MACS separation with and without TGF-β treatment (10 × magnification). (B) Percentage of CD44v9+ cells within the CD44std and CD44v9 cell subpopulations. (C) Western blot analysis of CD44 isoform expression in CD44std and CD44v9 cells. Representative images from three independent experiments, with the mean values and standard deviations. Significant differences are indicated by $*p < 0.05$; $**p < 0.005$, and $****p < 0.0001$.

proteins related to signaling. In CD44std cells after treatment with TGF-β, we found 58 proteins associated with signaling, 20 of which were associated with intracellular signal transduction, as determined by STRING (Supporting Information S1: Figure S3A). According to KEGG pathway analysis, several KEGG pathways were enriched in the upregulated proteins, such as ARHGEF11 (DOWN), MAPK3 (UP), CHD8 (DOWN), PLCB2 (Exclusive), PRKCA (UP), MAP2K7 (UP), MET (UP) and ITGA6 (DOWN). These proteins are significantly involved in different cancer-associated pathways, such as the ErbB, MAPK, PI3K-Akt, Wnt, VEGF and Ras pathways (Supporting Information S1: Figure 2A). In CD44v9 cells after treatment with TGF-β, we found 41 proteins participating in signaling, with 30 proteins related to intracellular signal transduction (Supporting Information S1: Figure S3B). These deregulated proteins included NFKB2, PRKAA1, MAPK1, MAPK13, MAPK3, DUSP16, RAPGEF2 and RASGRP3. The analysis revealed alterations in MAPK signaling, Rap1, VEGF, stem cell regulation, mTOR, Ras, pathways in cancer, and ErbB, TGF-β, PI3K-Akt and HIF-1 pathways (Figure 2B). By determining the abundance of the affected proteins in CD44std and CD44v9 cells after TGF-β treatment, a common trend emerged in the MAPK signaling pathway, characterized by elevated levels of MAPK3, PRKCA, MAP2K7, and MET in CD44std cells. On the contrary, CD44v9 cells exhibited a downregulation of the MAPK pathway, marked by alterations in the expression of NFKB2, MAPK1, MAPK3, MAPK13, DUSP16, RASGRP3 and RAPGEF2 (Figure 2C). These findings collectively indicate the differential activity of the MAPK signaling pathway between the CD44std and CD44v9 subpopulations.

3.3 | Validation of the Differential Alterations in the MAPK Signaling Pathway in CD44std and CD44v9 Cells After TGF-β Treatment

To confirm the observed differential alterations in the MAPK signaling pathway in CD44std and CD44v9 subpopulations following TGF-β treatment, WB analysis was conducted to validate the activation of key components of the MAPK signaling axis, including Src, MEK, MAPK, and p-MAPK (Figure 3). The results revealed increased activation of Src, MEK, MAPK, and p-MAPK in CD44std cells after TGF-β treatment. In contrast, CD44v9 cells exhibited a reduction in Src and MEK activation, with no significant changes in MAPK expression and a decreased level of p-MAPK following TGF-β treatment. These findings provide robust confirmation of the distinct signaling dynamics in Src, MEK, MAPK, and p-MAPK signaling between CD44std and CD44v9 cells after exposure to TGF-β.

3.4 | TGF-β Mediates Alterations in CSC Characteristics (Clonogenicity and Spheroid Formation) in the CD44std and CD44v9 Subpopulations

Given the observed differences in MAPK signaling between CD44std and CD44v9 cells, we sought to investigate potential modifications in CSC characteristics induced by TGF-β stimulation in these subpopulations. To assess these changes, we examined the expression of transcription factors associated with

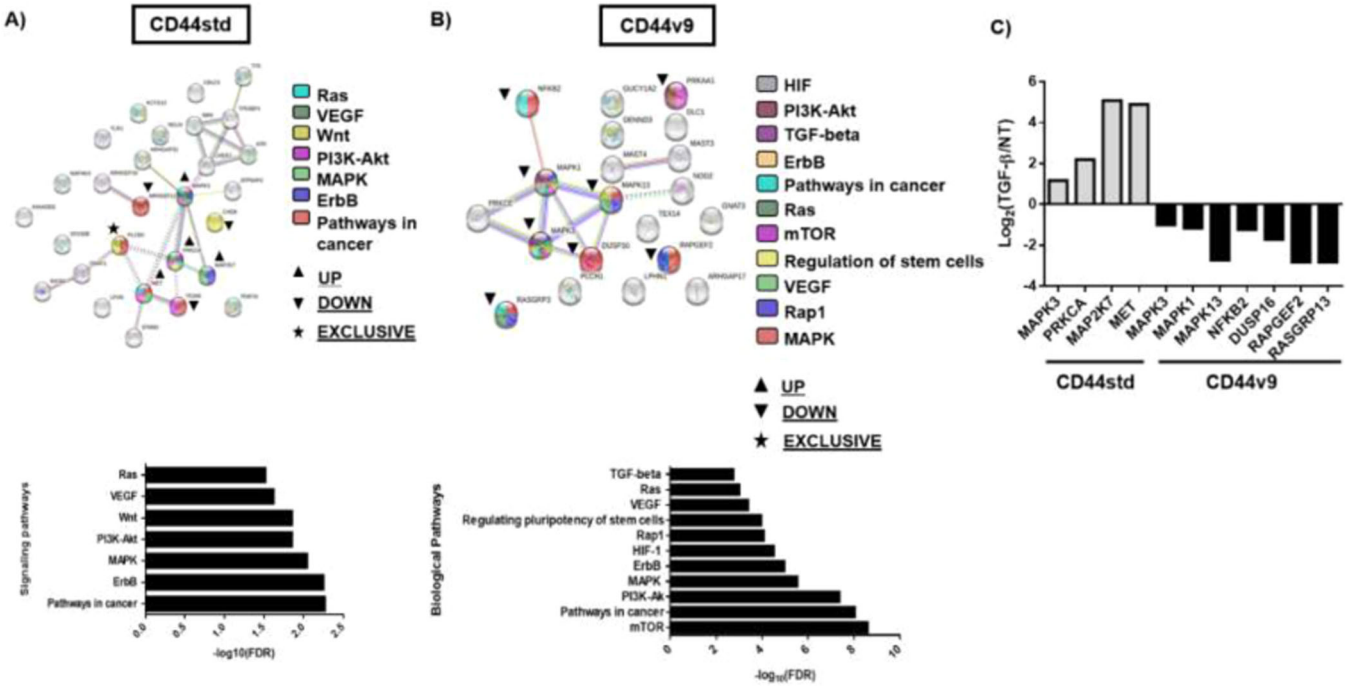

FIGURE 2 | Proteomic Analysis of Signaling in CD44std and CD44v9 Cells Following TGF-β Treatment. (A) Interaction network (constructed with STRING) of 30 proteins involved in the CD44std subpopulation after TGF-β treatment, highlighting predominantly upregulated proteins (MAPK3, PRKCA, MAP2K7, MET), downregulated proteins (ARHGEF11, CHD8 and ITGA6) and an exclusive protein (PLCB2). These proteins are involved in different signaling pathways (RAS, VEGF, Wnt, PI3K-Akt, MAPK, ErbB and pathways in cancer). (B) Interaction network (constructed with STRING) showing 20 proteins linked to CD44v9 after TGF-β exposure; all proteins exhibited downregulation (NFKB2, PRKAA1, MAPK1, MAPK3, MAPK13, DUSP16, RAPGEF2 and RASGRP3). These proteins are involved in different signaling pathways (MAPK, Rap1, VEGF, Regulating of stem cells, mTOR, Ras, Pathways in cancer, ErbB, TGF-β, PI3K-AKT and HIF-1). (C) Abundance graph of proteins (Log2(TGF-β/NT)) affected in upregulated and downregulated MAPK signaling present in CD44std (MAPK3, PRKCA, MAP2K7 and MET) and CD44v9 (MAPK3, MAPK1, MAPK13, NFKB2, DUSP16, RAPGEF2 and RASGRP13) cells, respectively.

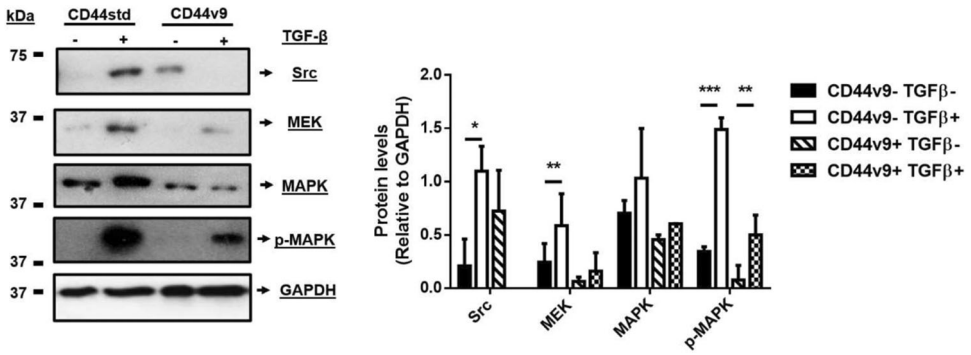

FIGURE 3 | Validation of Differential MAPK Signaling in the CD44std and CD44v9 Subpopulations Following TGF-β Treatment. Western blot analysis of Src, MEK, MAPK, and p-MAPK protein levels and densitometric quantification, employing GAPDH as a control. Representative images derived from three independent experiments, with data presented as the mean values ± standard deviations. Significance is indicated by $*p < 0.05$ and $**p < 0.005$.

pluripotency via WB analysis (Figure 4A). Both subpopulations exhibited a lack of Oct4 expression following TGF-β treatment. However, the expression of Sox2 and Nanog was detected in both subpopulations. Nanog was consistently expressed in CD44std cells, whereas its expression was less in CD44v9 cells after TGF-β treatment. Moreover, Sox2 expression was increased in CD44std cells but remained unchanged in CD44v9 cells after TGF-β treatment. Subsequently, the in vitro colony and spheroid formation capacities were assessed. The ability to form colonies and spheroids were enhanced in CD44std cells while attenuated in CD44v9 cells in response to TGF-β (Figure 4B,C). These results indicate an alteration in CSC characteristics in CD44std and CD44v9 cells following TGF-β treatment.

3.5 | TGF-β Amplifies Mesenchymal Traits, Invasion, and Migration in CD44std Cells and Adhesion in CD44v9 Cells

Subsequently, we examined the specific alterations in EMT characteristics induced by TGF-β exposure in CD44std and CD44v9 cells. Our analysis involved assessing the expression of

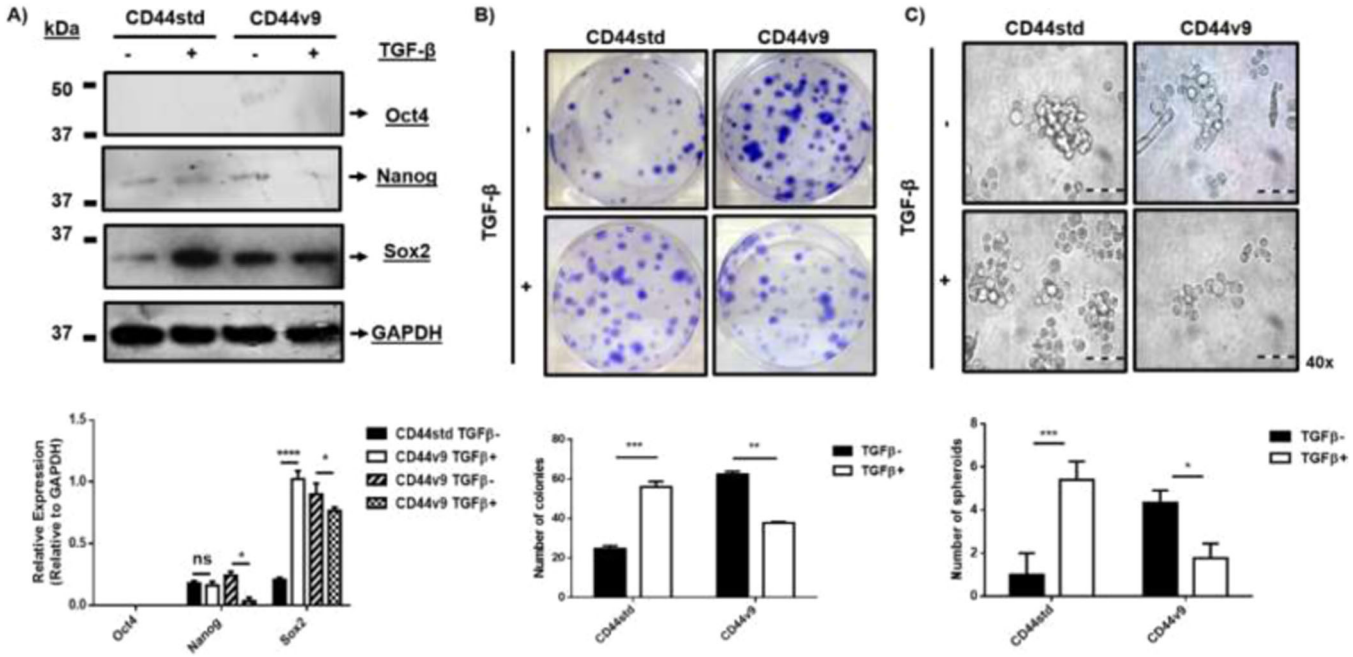

FIGURE 4 | Impact of TGF-β on CSC Transcription Factor Expression and Evaluation of Colony and Spheroid Formation in the CD44std and CD44v9 Subpopulations. (A) Western blot analysis of Oct4, Nanog, and Sox2 expression, with densitometric analysis, using GAPDH as a control. (B) Colony formation assay with the corresponding colony counts. (C) Micrographs (40× magnification) of spheroids and quantification of spheroid numbers. The scale bars represent 100 μm. Representative images from three independent experiments. Data are presented as the mean values ± standard deviations. Significance is indicated by $*p < 0.05$; $**p < 0.005$, and $****p < 0.0001$.

the EMT markers vimentin, N-cadherin, and E-cadherin by WB analysis. The results revealed a notable increase in the expression of vimentin and N-cadherin, as well as a reduction in E-cadherin expression, in both CD44std and CD44v9 cells (Figure 5A). Subsequently, we evaluated the functional aspects of the wound closure, invasion and adhesion processes. TGF-β treatment significantly increased the migratory and invasive potential of CD44std cells compared to CD44v9 cells (Figure 5B,C). In contrast, TGF-β stimulation significantly increased the adhesive capacity of CD44v9 cells relative to CD44std cells (Figure 5D). These data demonstrate the TGF-β-driven modulation of EMT in CD44std and CD44v9 cells, resulting in increased invasion and migration of CD44std cells and increased adhesion of CD44v9 cells.

4 | Discussion

One of the inducers of EMT is TGF-β, which serves as one of the catalysts to initiate EMT and has been associated with alterations in CD44 isoforms [13–15]. In this context, we observed a shift toward a mesenchymal morphology in both the CD44std and CD44v9 subpopulations, accompanied by a reduction in CD44v expression and maintenance of CD44std expression following exposure to TGF-β. From a molecular perspective, this TGF-β-induced transition from the CD44v isoform to CD44std has been associated with the involvement of SMAD3 and PCBP1, leading to increased migration, invasion, and tumorigenicity [16]. Moreover, ESRP1 has been identified as the principal regulator of posttranslational processing that maintains the epithelial phenotype, and ESRP1 suppression is initiated by TGF-β [13]. These findings suggest that potential molecular effectors such as SMAD3/PCBP1 or ESRP1 could be pivotal targets in explaining the isoform switch of CD44v to CD44std in the presence of TGF-β and help to determine the roles of these isoforms in HCC.

In the present study, several proteins related to the MAPK signaling pathway were identified. MAPK3 appears to be a pivotal protein, with its observed upregulation and downregulation converging in both the CD44std and CD44v9 subpopulations after exposure to TGF-β. This feature could make it an interesting target for regulation in both SNU-423 cells and the abovementioned subpopulations. MAPK3, also known as ERK1, is a kinase that is activated downstream of tyrosine kinase receptor in conjunction with ERK2. Since no independent studies have evaluated ERK1 separately, we discuss it as ERK1/2. Activation of ERK1/2 results from RAS, RAF, and MEK signaling, which activates processes such as proliferation, differentiation, cell cycle progression, and tumorigenesis. ERK1/2 activates proteins such as c-Myc, survivin, cyclin D1, metalloproteinases, and Bcl-2 [17]. Overexpression of ERK1/2 leads to uncontrolled proliferation and inhibition of apoptosis in various cancer types [18]. In HCC, constitutive MAPK signaling is maintained in approximately 50% of patients. This abnormal activation results from the overexpression of upstream growth factors and receptors (HGF and FGF) and downregulation of negative regulators (RAS-GAP) or positive modulators (RAS-GEF) of ERK1/2 [19]. Inhibition of ERK1/2 can disrupt proliferation, promote apoptosis, and stimulate differentiation, thus limiting tumor formation [20]. Reports on the downregulation and upregulation of proteins integrated into MAPK signaling have revealed multiple targets that may be involved in the changes observed in the CD44std and CD44v9

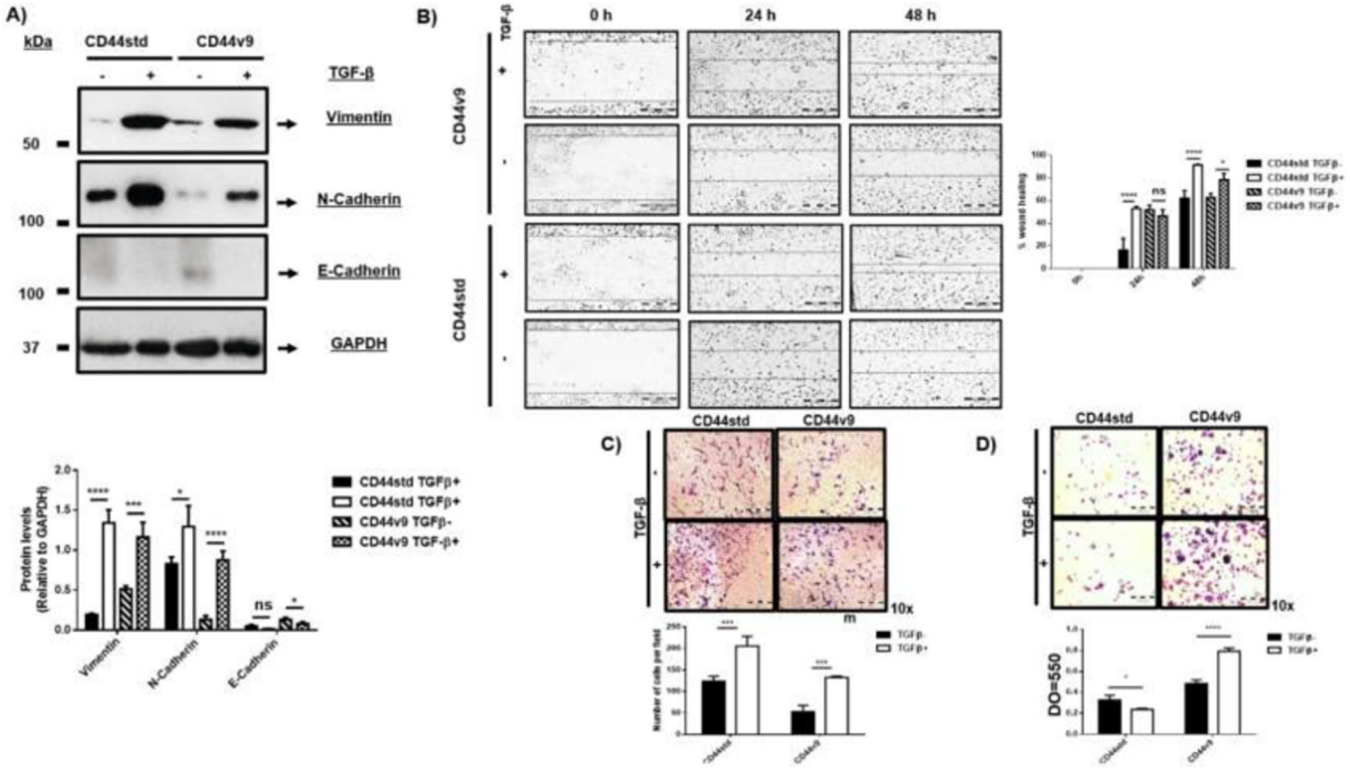

FIGURE 5 | The Impact of TGF-β on EMT Marker Expression and Assessment of Migration, Invasion, and Adhesion in CD44std and CD44v9 Subpopulations. (A) Western blot analysis of vimentin, N-cadherin, and E-cadherin expression in total protein lysates, with GAPDH serving as a control. (B) Wound healing assay with representative images captured at 0, 24, and 48 h; the scale bars represent 200 μm. (C) Invasion assay using a Boyden chamber, with representative images at 48 h (10× magnification) and cell counts in six fields of view. (D) Images of the fibronectin adhesion assay (10× magnification) and the corresponding absorbance measurements at 550 nm to evaluate cell adhesion. Representative images from three independent experiments. Data are presented as the mean values ± standard deviations. Significant differences are indicated by $^{*}p < 0.05$; $^{**}p < 0.005$, and $^{****}p < 0.0001$.

subpopulations under the influence of TGF-β. These data suggest that several upregulated and deregulated proteins integrated into MAPK signaling may be multiple targets that may be related to the changes observed in CD44std and CD44v9 subpopulations following TGF-β.

It has been established that the influence of TGF-β on total CD44 or CD44std expression enhances behaviors such as colony and spheroid formation, migration, and invasion during EMT [21, 22]. We found that the CD44std subpopulation did not exhibit changes in Nanog expression but showed an increase in Sox2 expression. In contrast, we observed an increase in Nanog but no change in Sox2 expression in the CD44v9 subpopulation. The mechanism by which TGF-β modifies CSC characteristics has been studied in various types of cancer. In breast cancer, TGF-β treatment was described to promote an increase in the expression of Oct4, Nanog, and mesenchymal markers in CSCs [23]. Additionally, in studies in which Slug, an effector of TGF-β, was silenced, it inhibited Nanog and Sox2 expression in vivo in HCC tumors [24]. Additionally, TGF-β has been shown to upregulate CD44 expression and induce EMT through the AKT/GSK3-β/β-catenin signaling axis, accompanied by acquisition of a CSC phenotype, in HCC cells [21]. Therefore, it is important to consider the silencing of Nanog or Sox2 in the CD44std and CD44v9 subpopulations after TGF-β treatment and how it affects the AKT, Hedgehog, or Wnt signaling pathway related to Nanog, Sox2, or Oct4. This consideration will help determine the relationship between the changes in the expression of transcription factors associated with pluripotency and the modulation of characteristics such as colony and spheroid formation abilities in the CD44std and CD44v9 subpopulations after stimulation with TGF-β. As expected, we observed increases in the N-cadherin and vimentin levels in both CD44std and CD44v9 cells following TGF-β stimulation. These changes are associated with migration and invasion, where we can see a direct relationship of spindle-like morphology after TGF-β. Interestingly, we noted that CD44v9 cells exhibited increased adhesion to fibronectin after exposure to TGF-β. It is possible that other components involved in the EMT process, such as Twist or Snail, may play a role in TGF-β mediated changes. Overexpression of Twist has been linked to the acquisition of CSC characteristics [25]. Loss of Snail induces EMT, thereby increasing spheroid formation in head and neck cancer cell lines [26]. These findings suggest that these EMT-related components may contribute to the acquisition of CSC traits in CD44std cells after TGF-β treatment. The influence of CD44 on cellular adhesion to fibronectin in the presence of TGF-β has not been reported. The literature mentions that TGF-β induces the colocalization of HA and fibronectin in myofibroblasts [27]. HA serves as a ligand, implying a potential connection between CD44 isoforms. This may imply a relationship between CD44 isoforms, HA synthesis, and the increase in TGF-β-mediated fibronectin adhesion, which would be a point of interest to explore in the future.

This constellation of alterations in CSC characteristics appears to be closely related to the crosstalk between MAPK and TGF-β. Such interplay has been previously described, where cross-signaling involving MAPK and TGF-β is essential for completion of the EMT process via a feedback loop involving autocrine TGF-β signaling. This mechanism includes the phosphorylation of SMAD coactivators by ERKs or the phosphorylation of SMAD2/3 by ERKs [28]. Conversely, inhibiting ERK1/2 activation has been shown to attenuate the tumor-promoting effect of TGF-β in cholangiocarcinoma [29]. Most of the available data establish a clear relationship among ERK1/2, TGF-β, and EMT. In this context, we can hypothesize that the differentially regulated proteins in the MAPK signaling pathway during EMT, in the context of differential CD44 isoform expression, may influence the acquisition or loss of CSC traits.

5 | Conclusion

In conclusion, it was observed that TGF-β modulates CSC traits in CD44 subpopulations. These results underscore the importance of proteomic analysis in the CD44std and CD44v9 subpopulations. The various proteins in the MAPK pathway identified in this study could serve as targets for further investigation, which would shed light on how these proteins might modulate the CSC characteristics (clonogenic/spheroid formation) and the EMT of these subpopulations and their role in HCC progression.

Author Contributions

Saúl Villa-Treviño and Carolina Piña-Vázquez were responsible for the study conception and work management. Mario Alejandro Aguilar-Chaparro, Sonia Andrea Rivera-Pineda and Hury Viridiana Hernández-Galdámez were responsible for conducting experiments and processing results. Mario Alejandro Aguilar-Chaparro, Emmanuel Ríos-Castro and Olga Lilia Garibay-Cerdenares were responsible for proteomic analysis. Mario Alejandro Aguilar-Chaparro was responsible for writing the main text. Mario Alejandro Aguilar-Chaparro and Saúl Villa-Treviño were responsible for discussion of the results and editing the manuscript.

Acknowledgments

The authors extend their gratitude to Eunice Romo Medina, Alejandro Cruz Hernández, Sergio Hernández García, Víctor Manuel Ortiz Santiago, and Victor Hugo Rosales for their contribution to the research group and for their support throughout the development of this project. Furthermore, we want to express our gratitude to CONAHCYT (70366) for providing a scholarship to Mario Alejandro Aguilar-Chaparro, wich facilitated the realization of this work.

Conflicts of Interest

The authors declare no conflicts of interest.

Data Availability Statement

The data that support the findings of this study are available from the corresponding author upon reasonable request.

References

1. H. Sung, J. Ferlay, R. L. Siegel, et al., "Global Cancer Statistics 2020: GLOBOCAN Estimates of Incidence and Mortality Worldwide for 36 Cancers in 185 Countries," *CA: A Cancer Journal for Clinicians* 71, no. 3 (2021): 209–249.

2. J. M. Llovet, R. K. Kelley, A. Villanueva, et al., "Hepatocellular Carcinoma," *Nature Reviews Disease Primers* 7, no. 1 (2021): 6.

3. S. Lotfollahzadeh, A. Recio-Boiles, and H. M. Babiker, Liver Cancer, in *StatPearls*. 2023.

4. A. R. Jordan, R. R. Racine, M. J. P. Hennig, and V. B. Lokeshwar, "The Role of CD44 in Disease Pathophysiology and Targeted Treatment," *Frontiers in Immunology* 6 (2015): 182.

5. L. Wang, et al, "The Role of CD44 and Cancer Stem Cells," *Methods in Molecular Biology* 1692 (2018): 31–42.

6. R. Azevedo, C. Gaiteiro, A. Peixoto, et al., "CD44 Glycoprotein in Cancer: A Molecular Conundrum Hampering Clinical Applications," *Clinical Proteomics* 15 (2018): 22.

7. K. Endo and T. Terada, "Protein Expression of CD44 (Standard and Variant Isoforms) in Hepatocellular Carcinoma: Relationships With Tumor Grade, Clinicopathologic Parameters, p53 Expression, and Patient Survival," *Journal of Hepatology* 32, no. 1 (2000): 78–84.

8. K. Mima, H. Okabe, T. Ishimoto, et al., "CD44s Regulates the TGF-β–Mediated Mesenchymal Phenotype and Is Associated With Poor Prognosis in Patients With Hepatocellular Carcinoma," *Cancer Research* 72, no. 13 (2012): 3414–3423.

9. K. Mima, H. Okabe, T. Ishimoto, et al., "The Expression Levels of CD44v6 are Correlated With the Invasiveness of Hepatocellular Carcinoma In Vitro, But Do Not Appear to Be Clinically Significant," *Oncology Letters* 3, no. 5 (2012): 1047–1051.

10. M. A. Aguilar-Chaparro, S. A. Rivera-Pineda, H. V. Hernández-Galdámez, C. Piña-Vázquez, and S. Villa-Treviño, "The CD44std and CD44v9 Subpopulations in Non-Tumorigenic Invasive SNU-423 Cells Present Different Features of Cancer Stem Cells," *Stem Cell Research* 72 (2023): 103222.

11. A. Hayakawa, M. Saitoh, and K. Miyazawa, "Dual Roles for Epithelial Splicing Regulatory Proteins 1 (ESRP1) and 2 (ESRP2) in Cancer Progression," *Advances in Experimental Medicine and Biology* 925 (2017): 33–40.

12. K. Mima, H. Hayashi, K. Imai, et al., "High CD44s Expression Is Associated With the EMT Expression Profile and Intrahepatic Dissemination of Hepatocellular Carcinoma After Local Ablation Therapy," *Journal of Hepato-Biliary-Pancreatic Sciences* 20, no. 4 (2013): 429–434.

13. H. Y. Zhang and K. F. Dou, "PCBP1 Is an Important Mediator of TGF-β-Induced Epithelial to Mesenchymal Transition in Gall Bladder Cancer Cell Line GBC-SD," *Molecular Biology Reports* 41, no. 8 (2014): 5519–5524.

14. Q. Chen, M. Gu, Z. Cai, et al., "TGF-β1 Promotes Epithelial-To-Mesenchymal Transition and Stemness of Prostate Cancer Cells by Inducing PCBP1 Degradation and Alternative Splicing of CD44," *Cellular and Molecular Life Sciences* 78, no. 3 (2021): 949–962.

15. J. Zhou, Y. Du, Y. Lu, et al., "CD44 Expression Predicts Prognosis of Ovarian Cancer Patients Through Promoting Epithelial-Mesenchymal Transition (EMT) by Regulating Snail, ZEB1, and Caveolin-1," *Frontiers in Oncology* 9 (2019): 802.

16. V. Tripathi, K. M. Sixt, S. Gao, et al., "Direct Regulation of Alternative Splicing by SMAD3 through PCBP1 Is Essential to the Tumor-Promoting Role of TGF-β," *Molecular Cell* 64, no. 3 (2016): 549–564.

17. C. Braicu, M. Buse, C. Busuioc, et al., "A Comprehensive Review on MAPK: A Promising Therapeutic Target in Cancer," *Cancers* 11, no. 10 (2019): 1618.

18. Y. J. Guo, W.-W. Pan, S.-B. Liu, et al., "ERK/MAPK Signalling Pathway and Tumorigenesis," *Experimental and Therapeutic Medicine* 19, no. 3 (2020): 1997–2007.

19. H. Moon and S. W. Ro, "MAPK/ERK Signaling Pathway in Hepatocellular Carcinoma," *Cancers* 13, no. 12 (2021): 3026.

20. R. Sugiura, R. Satoh, and T. Takasaki, "ERK: A Double-Edged Sword in Cancer. ERK-Dependent Apoptosis as a Potential Therapeutic Strategy for Cancer," *Cells* 10, no. 10 (2021): 2509.

21. N. R. Park, J. H. Cha, J. W. Jang, et al., "Synergistic Effects of CD44 and TGF-β1 through AKT/GSK-3β/β-Catenin Signaling During Epithelial-Mesenchymal Transition in Liver Cancer Cells," *Biochemical and Biophysical Research Communications* 477, no. 4 (2016): 568–574.

22. Y. Gao, B. Ruan, W. Liu, et al., "Knockdown of CD44 Inhibits the Invasion and Metastasis of Hepatocellular Carcinoma Both In Vitro and In Vivo by Reversing Epithelial-Mesenchymal Transition," *Oncotarget* 6, no. 10 (2015): 7828–7837.

23. D. Wang, P. Lu, H. Zhang, et al., "Correction: Oct-4 and Nanog Promote the Epithelial-Mesenchymal Transition of Breast Cancer Stem Cells and Are Associated With Poor Prognosis in Breast Cancer Patients," *Oncotarget* 12, no. 10 (2021): 1024–1025.

24. X. Zhao, B. Sun, D. Sun, et al., "Slug Promotes Hepatocellular Cancer Cell Progression by Increasing sox2 and Nanog Expression," *Oncology Reports* 33, no. 1 (2015): 149–156.

25. S. A. Mani, W. Guo, M. J. Liao, et al., "The Epithelial-Mesenchymal Transition Generates Cells With Properties of Stem Cells," *Cell* 133, no. 4 (2008): 704–715.

26. Y. C. Chen, Y. W. Chen, H. S. Hsu, et al., "Aldehyde Dehydrogenase 1 Is a Putative Marker for Cancer Stem Cells in Head and Neck Squamous Cancer," *Biochemical and Biophysical Research Communications* 385, no. 3 (2009): 307–313.

27. S. P. Evanko, S. Potter-Perigo, L. J. Petty, G. A. Workman, and T. N. Wight, "Hyaluronan Controls the Deposition of Fibronectin and Collagen and Modulates TGF-β1 Induction of Lung Myofibroblasts," *Matrix Biology* 42 (2015): 74–92.

28. L. Xie, B. K. Law, A. M. Chytil, K. A. Brown, M. E. Aakre, and H. L. Moses, "Activation of the Erk Pathway Is Required for TGF-β1-Induced EMT In Vitro," *Neoplasia* 6, no. 5 (2004): 603–610.

29. P. Sritananuwat, N. Sueangoen, P. Thummarati, K. Islam, and T. Suthiphongchai, "Blocking ERK1/2 Signaling Impairs TGF-β1 Tumor Promoting Function But Enhances Its Tumor Suppressing Role in Intrahepatic Cholangiocarcinoma Cells," *Cancer Cell International* 17 (2017): 85.

Supporting Information

Additional supporting information can be found online in the Supporting Information section.